Chapter 4

Controlled Drug Delivery using Functionalized Layered Double Hydroxides

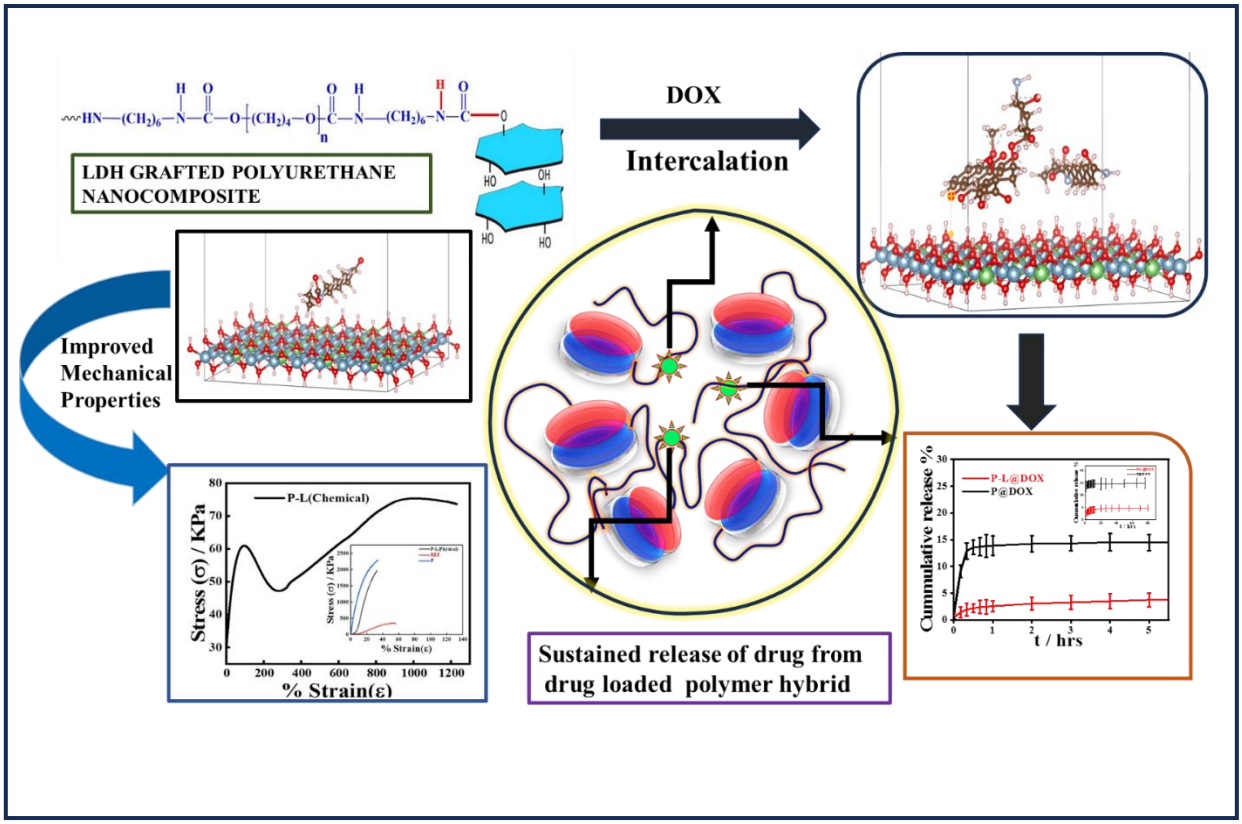

4.1. Introduction

According to the Global Cancer Observatory (GCO), cancer remains the leading cause of death globally, with its incidence and mortality increasing at a concerning rate. This rise is driven by the growing population size and aging demographics, compounded by escalating risk factors such as obesity, pollution, and changing dietary patterns over the years. In 2022, nearly 20 million new cancer diagnoses occurred, resulting in 10 million deaths. These alarming statistics indicate that nearly one in five individuals will develop cancer during their lifetime, with one in nine men and one in twelve women succumbing to this grave illness [1]. These circumstances highlight the urgent necessity for the advancement of more effective strategies to combat cancer. Despite ongoing research and initiatives to tackle this disease, the quest for new treatments remains paramount. While surgery, chemotherapy, and radiotherapy are established foundations in cancer care, each approach has its limitations, underscoring the need for improvement [2-3]. Although chemotherapy is a mainstay for treating most solid and hematological malignancies, the hypoxic conditions of the tumor microenvironment (TME) can swiftly lead to cancer cell resistance, causing treatment failure. Increasing dosages to counteract this resistance often results in severe side effects, including nausea, cardiotoxicity, appetite loss, myelosuppression, mucositis, alopecia, and liver dysfunction [4-5]. To address these issues, combining chemotherapy with other therapeutic modalities is often viewed as a promising strategy, allowing for reduced drug dosages without compromising overall efficacy, as the combined regimen introduces additional anticancer mechanisms [6]. The primary challenges lie in achieving effective cellular uptake and targeted delivery of anticancer agents. Despite advancements in drug-delivery systems, direct delivery often proves ineffective due to obstacles such as enzymatic degradation, low bioavailability, poor circulatory stability, and unfavourable accumulation of drug carriers [7]. The search for more effective anticancer therapies has

led to the creation of both viral and nonviral drug-delivery vectors designed to enhance cellular uptake into malignant cells. Targeted delivery methods are particularly sought after in cancer therapy, as they promise improved therapeutic and diagnostic efficacy with fewer side effects [8]. Researchers are also innovating sustained drug-release vehicles that address the limitations of traditional methods, enabling controlled drug release in response to stimuli or over time, thus prolonging the drug's presence in the bloodstream [9-11]. The intersection of modern biology, medicine, and nanotechnology has opened new, clinically relevant pathways for cancer treatment, transforming many conventional approaches to tumor management. In this context, inorganic-based nanoplatforms, noted for their versatile functionalities, enhanced quality control, and cost-effectiveness, are emerging as promising materials for advanced therapies [12-14]. However, a major challenge faced across all nanoparticle delivery routes is evading the immune system. Each route presents distinct physical barriers that must be navigated. For instance, oral delivery and inhalation pose specific challenges, while targeting specialized regions such as tumors or crossing the blood-brain barrier introduces additional complexities [15]. In recent years, polymer–inorganic nanocomposites have attracted considerable interest due to their ability to merge the strengths of both organic and inorganic materials. These hybrid systems offer the processing ease, flexibility, and damping capabilities typical of organic polymers while benefitting from the high strength, chemical resistance, and thermal stability afforded by inorganic components [16-17]. A critical factor in optimizing the performance of these nanocomposites is ensuring effective compatibility at the organic-inorganic interface, which largely hinges on the high dispersion of inorganic elements within the polymer matrix [18-21]. Various techniques, including in-situ polymerization and surface modification, have been developed to enhance the dispersion of inorganic nanoparticles. A notable approach employs cationic clays, such as montmorillonite, as nanofillers. This

method has significantly improved the mechanical properties of polymer-clay nanocomposites, demonstrating the potential of these hybrid materials in advancing modern materials science [22-23]. Nanocomposites made from polymers and inorganic fillers have captivated researchers for their unique preparation methods and remarkable properties, along with their promise for creating new hybrid materials tailored for specific applications within the realm of polymer composites. A novel class of inorganic materials, specifically LDHs, has been introduced as nanofillers in the development of polymer-based nanocomposites. LDHs are distinctive mixed metal hydroxides composed of different valent metal ions, crystallizing in a manner akin to mineral brucite, incorporating interlayer anionic species. Key aspects of characterizing these hybrid materials—such as morphological analysis and melt rheological behaviour—are thoroughly documented to illustrate how the dispersion of LDH particles affects the melt flow properties of the resulting nanocomposites. An exceptional feature of LDHs as nanofillers is their thermal decomposition behaviour, which makes them highly effective flame retardants for polymers. The synthesis of LDHs, along with their organic modifications and incorporation into polymer/LDH nanocomposites, has been extensively explored in recent studies. LDH represents a significant family of anionic functional materials. Their two-dimensional geometries resemble those of layered silicates, showcasing ultrathin platelets with a high aspect ratio. These structures can be represented by an idealized formula: $[M^{II}_{1-x}M^{III}_{x}(OH)_2]^{x+}[(A^{m-})_{x/m} . n(H_2O)]^{x-}$, where M^{II} and M^{III} represent divalent and trivalent metal ions, respectively, and A^{m-} is the interchangeable interlayer anion. While the combination of M^{II}-M^{III} LDH is well-documented in literature, Li-Al based LDHs nanocarriers stand as the sole known example of LDHs. Extensive studies have analyzed their free energy, structure, and anion intercalation. The diverse precursors utilized in their synthesis grant LDHs impressive versatility, allowing for fine-tuning of properties across a wide range of

applications - from catalysis, hydrogenation, and ion exchange to flame retardation and roles as biological carriers. When incorporated into polymer matrices, LDH nanoparticles can be introduced directly without modification or enhanced via coupling agents. Additionally, their eco-friendly nature stems from straightforward synthetic processes, high purity, and compatibility with various organic anions like carboxylates, sulfonates, and phosphates. This adaptability in chemical composition, combined with numerous interactions, optimizes dispersion when hybridized within polymers, making them invaluable in advanced materials science. Grafting synthetic polymers onto inorganic clays, LDHs, and backbones offers a versatile method for creating materials with enhanced functional properties, positioning them as ideal candidates for drug delivery systems. The structure and composition of these polymers are vital in regulating drug release through a diffusion mechanism. Among various techniques, chemical grafting emerges as an effective means of modifying the structure and properties of inorganic clay. In particular, graft polymerization of inorganic clay has become essential for developing advanced materials, significantly enhancing the functional properties of these inorganic clays and LDHs. One noteworthy innovation is the creation of graft copolymers that combine starch derivatives with methyl methacrylate (MMA) polymers, developed as direct compression excipients [24]. Under compression, these materials form porous matrix networks capable of regulating the release of model drugs, such as anhydrous theophylline, through diffusion. Furthermore, polyurethanes (PUs) represent a remarkable class of synthetic polymers due to their biodegradable and biocompatible characteristics, making them valuable in drug delivery systems and for their shape memory properties [25-27]. Their molecular design is easily adjustable by varying the hard and soft segments, including diisocyanates, diols, and chain extenders. Beyond traditional uses, ongoing research into biodegradable PUs for biomedical applications - such as temporary scaffolds, controlled release of active

ingredients, and ligament reconstruction prostheses - continues to advance. Hydrophilic poly (ethylene oxide)-based PU hydrogels have shown promising properties for drug delivery applications [31-32]. Grafting polyurethanes onto LDHs could represent a new frontier, creating a biodegradable and biocompatible polymer suitable for drug delivery, effectively balancing hydrophobic wrapping with hydrophilic moieties [33]. The choice of HMDI and PTMG in this study is primarily motivated by their wide commercial availability as essential raw materials, presenting significant potential for broadening industrial applications in the development of novel polymer/LDH nanocomposites. This led us to investigate the intriguing synergistic effects of interlamellar grafting and organomodification of LDHs within a polyurethane (PU) matrix. Our study focuses on how these modifications impact the morphology, interactions, mechanical properties, and thermal stability of the resulting nanocomposites, comparing these results with PU nanocomposites produced using either grafted or organomodified LDH alone [34].

4.2 Results and discussions

4.2.1. Designing of the tumor targeting polyurethane grafted Li-Al based LDH nanocomposite with thermal stability:

The hydrophilicity of the LDH framework is skilfully modified by incorporating hydrophobic polyurethane, ensuring a careful degree of grafting to achieve a desirable balance. As depicted in Scheme 1, the synthesis of the prepolymer followed by its grafting establishes an equilibrium between hydrophilic and hydrophobic characteristics. The polyurethane chains form covalent bonds with the LDH backbone through a reaction between the isocyanate-terminated prepolymer and the hydroxyl groups present in the

LDH, resulting in a stable urethane linkage (−NHCOO−). This intricate process allows for controlled modification of the material's properties.

To investigate the grafting of polyurethane onto the Li-Al based LDH backbone, ^{1}H NMR spectroscopy was performed, recording spectra in d-DMF for two samples: polyurethane (P) and the polyurethane-grafted Li-Al based LDH nanocomposite (P-L) **(Fig 4.1.a)**. The primary aim of this analysis was to validate the grafting of the LDH matrix and assess its impact on the chemical environment of the LDH. In the spectrum for P, a notable peak at 7.11 ppm corresponds to protons within the urethane linkage, indicating the presence of urethane bonds between poly(tetramethylene glycol) (PTMG) and 1,6-hexamethylene diisocyanate (HMDI). Following the grafting process, this peak shifts slightly to 7.21 ppm in the P-L spectrum.[35] Peaks at 4.37 ppm and 4.01 ppm correspond to protons in the PTMG segments, confirming the presence of glycol units in the polymer chain. Aliphatic protons in the polymer backbone are evident at 3.13 ppm, 2.28 ppm, and 2.12 ppm, likely reflecting the alkyl chains, while a peak at 0.95 ppm is linked to aliphatic groups in the matrix.

Conversely, the P-L spectrum shows a prominent peak at 9.90 ppm **(Figure 4.1.a)**, attributed to the -NH proton in the polyurethane linkage formed between the LDH and the prepolymer, marking a crucial sign of grafting that is absent in the PU spectrum. New peaks appear at 6.92 ppm, 6.60 ppm, and 6.23 ppm, suggesting further transformations in the polymer matrix following grafting. The shifts in aliphatic proton peaks to 2.26 ppm and 2.13 ppm indicate the influence of prepolymer grafting on the LDH backbone, while the peak at 0.95 ppm remains stable, indicating minimal influence from grafting in that region. Overall, the observed shifts and the emergence of new peaks substantiate the successful

grafting of LDH onto the polyurethane matrix, with distinct changes reflective of the degree of LDH incorporation.

The ^{13}C NMR NMR spectra provide additional insights into the chemical environment of the LDH post-grafting with polyurethane. For the prepolymer (P), distinct peaks appear at 70, 60, and 40 ppm, correlating with the carbon environments characteristic of the polyurethane backbone(Fig 4.1.b); the peaks at 70 and 60 ppm are attributed to alkylene glycol segments, while the peak at 40 ppm corresponds to the carbonyl carbons within the polyurethane chain. After grafting with LDH to create P-L, the spectrum becomes more complex, featuring new peaks at 157, 130, 117, 71, 64, 61, 41, and 20 ppm. The peak at 157 ppm is particularly significant, indicating the carbonyl carbon of the urethane linkage formed between the -OH group of the LDH and the -NCO group of the prepolymer. The peak at 71 ppm likely corresponds to hydroxyl groups in the LDH structure, while peaks at 64 and 61 ppm suggest interactions between the polyurethane and the Li-Al based LDH nanocarrier. Noteworthy shifts in peaks and new signals at 126 and 117 ppm indicate a higher degree of grafting and stronger interactions between the LDH and polyurethane. The peak at 157 ppm points to subtle modifications in the LDH environment, possibly due to increased interactions or structural changes within the LDH.

The degree of substitution in the nanocomposite matrix was quantified through NMR analysis, revealing a substitution level of 48% for the P-L composite, indicating a significant grafting of the prepolymer into the LDH matrix. This finding underscores that greater grafting levels can enhance the material's mechanical strength, thermal stability, and other desirable properties, depending on its intended applications.

FTIR spectroscopy of polyurethane (P), the nanocomposite (P-L), and the doxorubicin-loaded nanocomposite system (P-L@Dox) provides in-depth insights into their chemical

compositions and interactions. The FTIR spectrum of polyurethane (P) shows several key peaks, including a characteristic peak at 1100 cm^{-1} related to C-O stretching vibrations, which indicates ether linkages within the polymer backbone. The peak at 1371 cm^{-1} arises from C-H bending vibrations, while a significant peak at 1620 cm^{-1} corresponds to C=O stretching vibrations of the urethane group, confirming the formation of the polyurethane structure. Peaks at 2850 cm^{-1} and 2940 cm^{-1} correspond to the C-H stretching vibrations of aliphatic chains, and the broad peak at 3480 cm^{-1} reflects O-H stretching, likely from residual hydroxyl groups or moisture absorption, along with the signature of a free -NH group. A peak at 3340 cm^{-1} indicates hydrogen-bonded -NH groups, characteristic of polyurethane linkages. [36]**(Figure 4.1.c)**

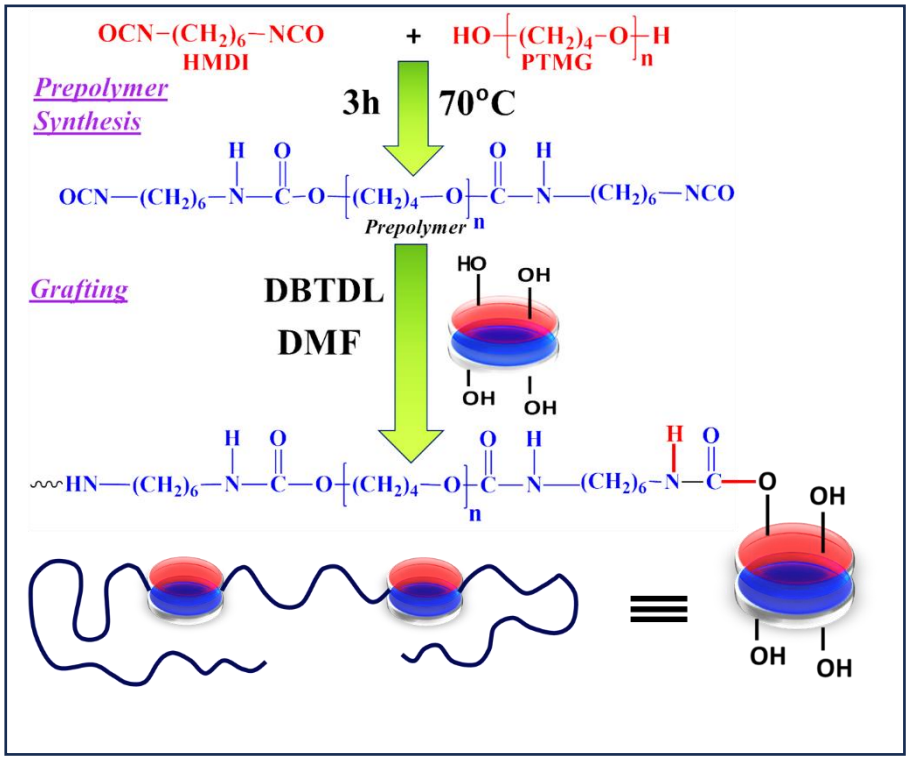

Scheme 1: Synthetic Scheme of PU grafted LDH (P-L)

In the case of pristine LDH (L), its FTIR spectrum displays distinct peaks, such as those at 733 cm^{-1} and 1005 cm^{-1}, associated with metal-oxygen vibrations within the LDH structure. The peak at 1366 cm^{-1} indicates the bending vibrations of hydroxyl groups, while

the peak at 1622 cm^{-1} corresponds to the bending of interlayer water molecules or hydroxyl groups within the LDH structure. A broad peak at 3421 cm^{-1} is characteristic of O-H stretching vibrations.[40] The FTIR spectrum of the grafted LDH nanocomposite (P-L) integrates features from both the polyurethane and LDH, with peaks at 745 cm^{-1} and 995 cm^{-1}, along with the C-O stretching peak at 1100 cm^{-1}, suggesting the successful incorporation of LDH into the nanocomposite system. The peak at 1374 cm^{-1} corresponds to C-H bending vibrations, and a new peak at 1717 cm^{-1} indicates the presence of carbonyl groups introduced via grafting interactions. The peaks at 2863 cm^{-1} and 2948 cm^{-1} demonstrate that the polyurethane structure remains largely intact, while the 3330 cm^{-1} peak signifies the formation of polyurethane linkages between the LDH's hydroxyl groups and the prepolymer's -NCO groups.

For the physical mixture of LDH and polyurethane (P-L physical), the FTIR spectrum reveals peaks at 745 cm^{-1} and 995 cm^{-1} indicative of the LDH structure, and peaks at 3337 cm^{-1} and 3417 cm^{-1}, reflecting structural similarities with the prepolymer P. However, the grafted system exhibits a single peak at 3330 cm^{-1}, representing the polyurethane linkage between LDH and the prepolymer, distinguishing P-L (chemical) from P-L (physical). This differentiation in FTIR peaks serves as a clear indicator of whether the polyurethane is incorporated into the layered double hydroxide matrix physically or chemically.

The FTIR spectra also elucidate the interactions between doxorubicin (Dox) and the various matrices of polyurethanes and LDHs. For pure Dox, peaks at 1730, 2905, and 3320 cm^{-1} are noted, with the 1730 cm^{-1} peak corresponding to the carbonyl group and the 3320 cm^{-1} peak reflecting OH stretching, reaffirming the drug's characteristic signatures. In the spectrum of Dox-loaded polyurethane (P@ Dox), peaks at 740, 1000, 1105, 1368, 1605, 2857, and 2940 cm^{-1} appear, harmonizing with the characteristic bands of both the

polyurethane matrix and the encapsulated Dox. Notably, the peaks at 1368 and 1605 cm^{-1}, attributed to aromatic ring vibrations of Dox, confirm its presence within the polyurethane structure. The peaks at 2857 and 2940 cm^{-1} relate to the aliphatic C-H stretching vibrations, reflecting the contributions from the polymer.

In contrast, the FTIR spectrum of Dox intercalated into the Li-Al based LDH system (L@Dox) displays peaks at 738, 1010, 1365, and 1605 cm^{-1}, where the presence of Dox is similarly confirmed by the peaks at 1365 and 1605 cm^{-1}. The FTIR spectrum of P-L@Dox reveals peaks at 740, 1000, 1107, 1378, 1705, 2861, 2940, and 3338 cm^{-1}. The prominent peak at 1705 cm^{-1} indicates carbonyl stretching vibrations, likely signifying the interaction between Dox and the LDH matrix. Additionally, the broad peak at 3338 cm^{-1} points to hydrogen bonding interactions involving Dox and the LDH nanocarrier. Collectively, the IR spectra illustrate how the spectral fingerprints of Dox are both retained and subtly modified within different matrices, underscoring the successful integration of the drug and its interaction with the polyurethane and LDH components.

The UV absorbance peaks for polyurethane (P) and the grafted material (P-L) are found at 288 nm and 293 nm, respectively.**(Figure 4.1.d)** LDH typically exhibit absorbance wavelengths ranging from 240 to 300 nm[37], indicating intrinsic electronic transitions within the LDH structure, often linked to metal-oxygen or metal-hydroxide interactions in the layered framework. The transition from 288 nm (P) to 293 nm (P-L) signifies a noteworthy interaction between the LDH and the polyurethane matrix, attributed to changes in the local electronic environment surrounding the LDH post-grafting. The interaction between the hydroxyl (-OH) groups of the LDH and the isocyanate (-NCO) groups of the polyurethane likely modifies the electronic transitions within the LDH, leading to this shift in the absorption peak. The difference in the UV peak of P-L compared to both pure LDH

and the polyurethane prepolymer implies that grafting introduces new interactions or modifies the electronic structure of the LDH. In contrast, the UV-Vis peak for the physical mixture of the prepolymer and LDH (P-L physical) appears at 287 nm, closely resembling the peak of pure P at 288 nm. This similarity suggests that the electronic transitions and structure of P and P-L (physical) are alike, reinforcing the idea that successful grafting in P-L (chemical) leads to distinct changes in the polyurethane backbone.

In the UV-Vis spectrum of doxorubicin (Dox), the pure drug shows a characteristic peak at 267 nm, corresponding to the π-π* transitions of its aromatic rings, along with absorption peaks in the 200-300 nm range [38]. The spectrum of Dox-loaded polyurethane (P@Dox) displays a slight red shift to 270 nm, indicating a change in the electronic environment of Dox due to interactions with the polyurethane matrix, potentially through hydrogen bonding or other forms of interaction with the polymer chains. For the Dox intercalated into the polyurethane grafted Li-Al based LDH nanocomposite (P-L@Dox), the UV-Vis spectrum reveals a peak at 266 nm, closely matching that of pure Dox, suggesting that the interaction between Dox and the grafted LDH nanocomposite does not significantly alter the drug's electronic structure.**(Figure 4.2.a)** However, a substantial shift is noted in the UV peak of Dox loaded onto pure LDH (L@Dox), appearing at 290 nm, indicating a strong interaction between Dox and the LDH layers, potentially involving charge transfer or significant alterations to the drug’s local electronic environment.

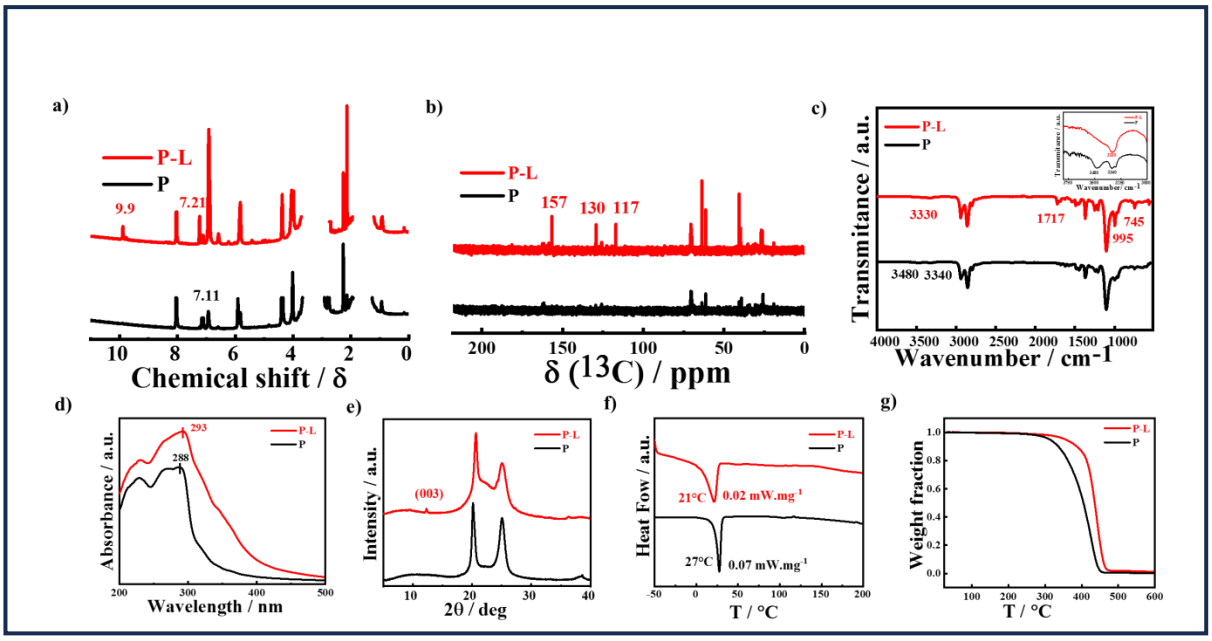

Figure 4.1: Evaluation of polymeric chain interactions and grafting with Li-Al based LDH nanocomposite. **a)** The ^{1}H NMR spectra of polyurethane prepolymer (P), and grafted derivative (P-L) reveal significant changes in hydrogen bonding, and the emergence of a new peak, at 9.9 ppm indicating successful grafting; **b)** The ^{13}C NMR spectra of P and P-L of the grafted counterparts further confirm the graft reaction with the appearance of a distinct new peak, additional detailed NMR peak information can be found in the Supplementary Information; **c)** FTIR spectra of the prepolymer (P) and graft nanocomposite (P-L) exhibit shifts in peak positions, underscoring the molecular interactions involved in the grafting process. In the FTIR spectrum, a distinct inset plot showcases the wavenumber range between 4000 and 3000 cm^{-1}, clearly highlighting the successful grafting of the chemical reaction between polyurethane and the Li-Al-based LDH nanocarrier (L). This interaction signifies the formation of a novel nanocomposite (P-L), demonstrating the effectiveness of the process; **d)** In comparison illustration of the solid state UV-Vis spectra of the prepolymer (P) and nanocomposite (P-L) that are indicated; **e)** Comparative X-ray diffraction analysis of prepolymer and nanocomposite (P-L); **f)** The DSC thermograms for P and P-L show the values for the melting point and heat of fusion,

g) TGA thermograms demonstrating the relative temperature stability of prepolymer (P) and novel grafting nanocomposite.

The structure of LDH has been thoroughly analyzed using powder XRD , revealing three distinct crystalline planes: (003), (006), and (009), alongside two well-separated peaks at (110) and (113). The crystalline domain size, calculated through the Debye-Scherrer equation, is determined to be 40 nm, with a corresponding d-spacing of 0.74 nm. In the XRD analysis, the polyurethane prepolymer (P) exhibits characteristic peaks at 20.2° and 24.9°[54] **(Figure 4.1.e) ,** indicating its crystalline nature. However, upon grafting with the Li-Al based LDH system to form the P-L nanocomposite, the XRD pattern experiences significant changes. The emergence of a new peak at 12.5° indicates successful grafting of LDH nanostructures onto the polyurethane matrix, suggesting that the LDH has intercalated into the polymer structure. This sharp peak, absent in the prepolymer, signifies the formation of new crystalline phases, likely stemming from the unique layered structure of LDH, which directly influences the diffraction pattern. These findings imply that LDH particles are well-dispersed within the polyurethane matrix, leading to the development of new crystalline structures and a modification of the composite's overall crystallinity. Such interactions provide valuable insight into how incorporating polyurethane into the LDH backbone alters the structural properties of LDH, with potential implications for various applications. For the P-L composite, the crystalline domain size and d-spacing are found to be 29 nm and 0.71 nm, respectively. This reduction in domain size suggests that the grafting process, which involves the reaction of LDH with the polyurethane prepolymer, impacts the structural integrity of the LDH. The integration of the polyurethane matrix appears to disrupt the regular stacking of the LDH layers, reducing the coherence length of the crystalline domains. The decreased d-spacing further indicates that grafting LDH within the polyurethane matrix leads to a more compact arrangement, likely facilitated by

interactions between the LDH hydroxyl groups and the NCO groups of the prepolymer, promoting closer packing of the LDH within the polymer chains. The incorporation of doxorubicin (Dox) into both P and P-L reveals intriguing differences in crystallinity. While P@Dox retains its original peaks at 20° and 24.5°, P-L@Dox exhibits a broader peak at 20° and a new crystalline feature at 11.5°, suggesting that Dox affects the crystalline structure of the P-L nanocomposite. The crystalline domain size, calculated using the Debye-Scherrer equation, is 35 nm compared to the pristine LDH, showing a reduction to 35 nm when grafted with polyurethane into the LDH matrix and loaded with Dox (P-L@Dox). While the drug loading may influence this alteration, the primary cause of the observed decrease is attributed to structural modifications resulting from the grafting process. These modifications reflect changes in the microstructural characteristics of the LDH material. The broadening and shifting of the peaks likely arise from drug incorporation, leading to structural changes that reduce crystallinity and may introduce new crystalline or amorphous phases. These findings underscore the significant influence of drug loading and LDH grafting on the structural properties of the polyurethane matrix, emphasizing the delicate interplay between crystallinity and material modifications [55].

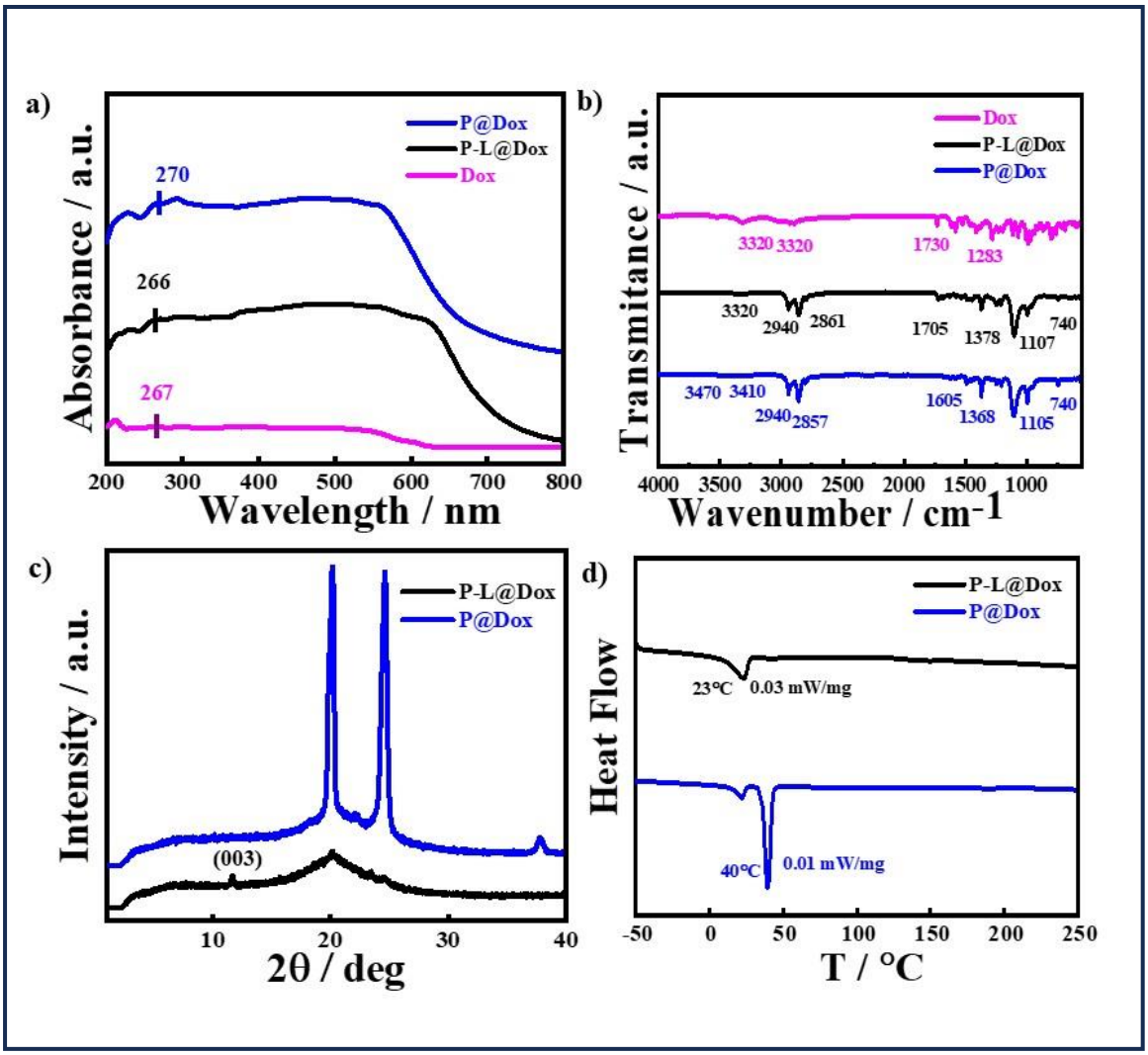

Figure 4.2: a) Uv-Vis spectra pure Dox, Dox loaded P and Dox loaded P-L. **b)** FTIR spectra pure Dox, Dox loaded P and Dox loaded P-L .**c)** X-ray diffraction analysis of Dox loaded P and Dox loaded P-L. **d)** The DSC thermograms for Dox loaded P and Dox loaded P-L

DSC was employed to investigate the thermal behavior of the nanocomposite, both with and without drug loading, in order to assess the effects of drug incorporation and interaction with Li-Al based LDH along with the nanocomposite. The pristine polyurethane (P) exhibited a prominent endothermic peak at 27°C with an enthalpy change of 0.07 mW/mg.(Fig 4.1.f) This peak signifies a glass transition temperature or phase shift within the polymer, most likely the melting of the soft segment[40], reflecting a fundamental thermal property of pure polyurethane. The introduction of polyurethane into the Li-Al

based LDH matrix, resulting in the grafted material P-L, led to the appearance of two distinct endothermic peaks at 21°C**(Figure 4.1.f),** accompanied by a reduced enthalpy change of 0.02 mW/mg. The shift in the glass transition temperature suggests that LDH influences the thermal properties of the polyurethane, likely affecting its structure and dynamics. The decrease in enthalpy change in P-L compared to P indicates that LDH may reduce the degree of crystallinity or alter the phase separation within the polymer matrix. The DSC profile of the LDH-modified, drug-loaded nanocomposite (P-L@Dox) displayed a single endothermic peak at 23°C **(Figure 4.2.d)**, indicating that LDH alters the interaction between Dox and the polymer, consequently modifying the thermal behaviour of the drug-loaded system. This highlights the influence of both drug incorporation and LDH on the thermal properties of polyurethane, offering insights into the stability, interactions, and potential applications of these materials in drug delivery systems.

The increase in degradation temperature observed through TGA of the polyurethane grafted nanocomposite system (P-L), compared to pure polyurethane (P), can be attributed to several key factors involving the chemical and physical interactions between the polyurethane matrix and the Li-Al based LDH. Initially, the pure polyurethane prepolymer (P) undergoes a single-stage degradation process at approximately 311°C, known as the degradation temperature where 5% of the sample's weight is lost in an inert atmosphere. This degradation primarily results from the cleavage of urethane linkages and the breakdown of the polymer backbone under thermal stress. The thermal stability of P is defined by the robustness of these linkages and the inherent structural integrity of the polymer. Upon grafting with polyurethane into the Li-Al based LDH matrix, forming P-L, the degradation temperature notably increases to 354°C. **(Figure 4.1.g)**This shift can be attributed to the formation of covalent bonds between the isocyanate (NCO) groups of the polyurethane prepolymer and the hydroxyl (OH) groups on the LDH. These covalent bonds

foster additional cross-linking within the polymer matrix. The enhanced cross-linking strengthens the polymer network, demanding higher energy to disrupt the chemical bonds and initiate degradation. Essentially, this is due to the intercalation or wrapping of polyurethane within the interlayer cavities of the LDH [41], similar to other grafting processes. Known for their thermal resistance, LDHs can act as a heat barrier. As the temperature rises, LDH may stabilize the polymer matrix by functioning as a heat sink or barrier, slowing the thermal decomposition of polyurethane chains. Despite both materials exhibiting single-stage degradation, the higher degradation temperature of P-L signifies that the LDH not only reinforces the polymer's structural integrity but also enhances its thermal endurance. This interaction highlights how grafting of organic prepolymer into inorganic materials (LDH) can significantly elevate their thermal stability and properties, providing valuable insights into developing more resilient polymeric materials.

4.2.2 Morphological understanding of prepolymer grafted Li-Al based LDH nanocomposite:

To investigate the morphological behavior of the nanocomposites, we employed advanced imaging techniques such as HRTEM, FESEM, AFM, and optical microscopy

Figure 4.3.a is HRTEM images of P-L nanocomposite. In these images, the greyish-white regions represent the polyurethane matrix, while the black regions indicate the Li-Al based LDH layers. The Li-Al based LDH layers appear highly dispersed throughout the polymer matrix, suggesting a partially exfoliated state in the nanocomposites and these findings suggest that the polymer chains penetrate into the interlayer regions of Li-Al based LDH, facilitating the exfoliation of the metal hydroxide sheets from one another.

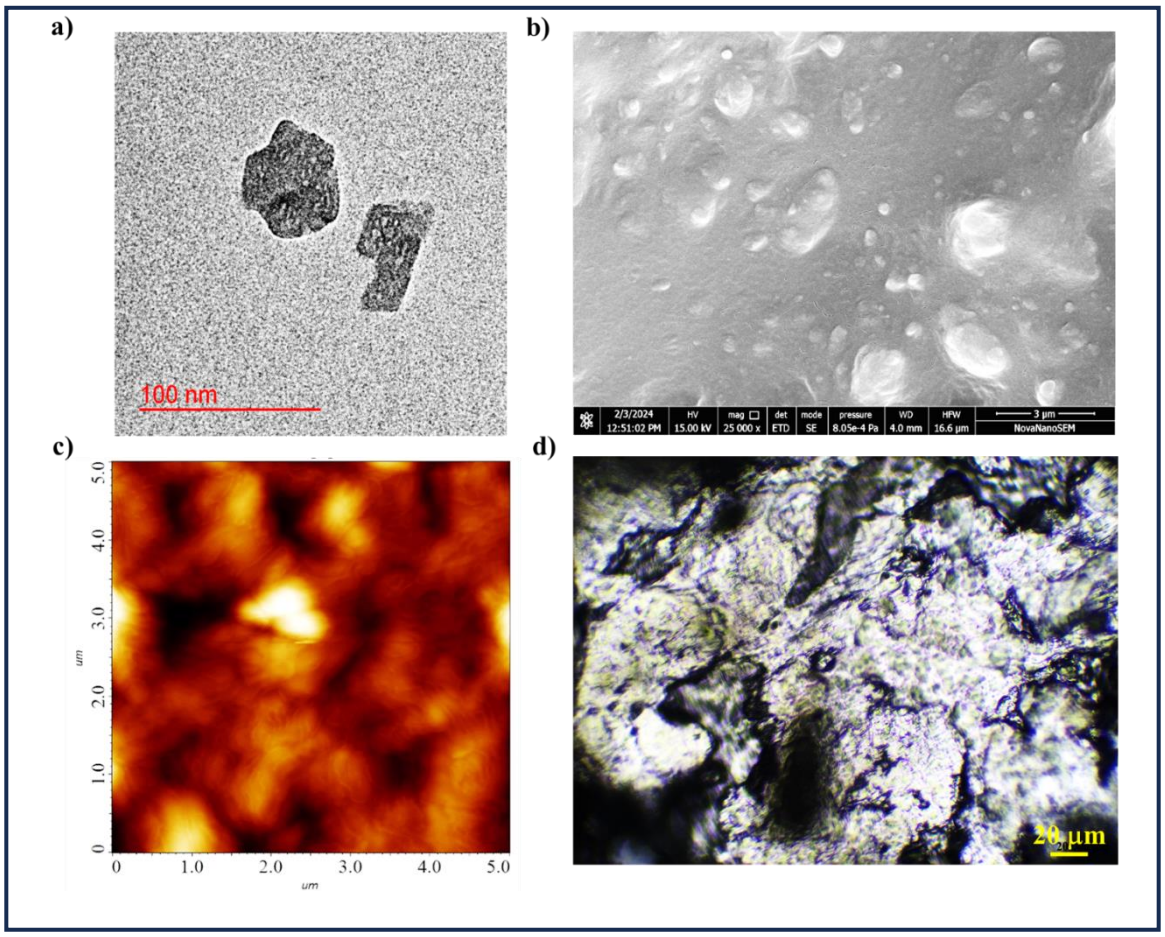

Figure 4.3: Polyurethane prepolymer grafted Li-Al based LDH nanocomposite (P-L) morphological behaviour, **a)** HRTEM microscopic image of P-L; **b)** HRSEM images of nanocomposite P-L; **c)** AFM images in semi-contact mode (5 × 5 μm^2) of P-L nanocomposite, **d)** Greater agglomerates can be seen in the nanocomposite (P-L) optical picture

To further investigate the dispersion of Li-Al based LDH within the polyurethane matrix, and to compare the interfaces of the prepolymer and the nanocomposite, FESEM was utilized to examine the freshly cut surfaces of polyurethane/LDH nanocomposites **(Figure 4.3.b).** The images display well-dispersed distorted hexagonal platelets within the polyurethane matrix, indicating that LDH nanoparticles serve as effective nanofillers. Polyurethane naturally tends to form aggregates through hydrogen bonding occurring between the hard and soft segments of its segmented polymer chains. In contrast, the graft density of the nanocomposite leads to a smaller blob size, a result of strongly correlated systems dominated by both intra- and intermolecular hydrogen bonding; these crystallite assemblies further agglomerate, resulting in a strip-like morphology. The segmented regions in the nanocomposite exhibit a higher contrast, closely resembling the pure prepolymer. This pronounced difference largely arises from the significant hydrogen bonding in the grafted nanocomposite, making them comparable to pure prepolymer. The extensive grafting of the prepolymer results in the formation of hard domain self-assemblies, driven by intermolecular hydrogen bonding between >C=O and >N–H groups, leading to notable microstructural changes. This increased inhomogeneity is further confirmed through optical images, where the larger dimensions of agglomerates in P-L are

evident compared to the prepolymer. Understanding self-assembly in the nanocomposite, these strip sizes accumulate into micro-clusters measured in optical images. This systematic self-assembly, progressing from the nanometre to micrometre scale, is primarily driven by hydrogen bonding originating from the polar groups in the LDH inorganic nanocarrier and the side-chain of the prepolymer. Such a bottom-up construction of self-assemblies presents a promising approach for biomaterials capable of binding biologically active molecules or drugs, which can be released in a controlled, sustained manner for more effective disease management. Furthermore, the thermal and mechanical properties of these organic-inorganic nanocomposites can be finely adjusted by varying the graft density, making them highly suitable as drug-delivery vehicles. The surface topology and crystalline structure, supported by FESEM and XRD data, further reinforce the insights presented here.

4.2.3. Mechanical, dynamical, and rheological behavior of the nanocomposite:

The schematic illustrates the mechanical response of a nanocomposite formed by the reaction between inorganic LDH nanocarriers and polyurethane, showcasing both chemical and physical experimental validations. Polyurethane, known for its adaptable mechanical properties and biocompatibility, holds significant potential for biomedical applications. The polyurethane grafted with Li-Al LDH, referred to as P-L, has been meticulously analyzed in comparison to both a reference polyurethane (REF), synthesized via the reaction between PTMG and HMDI with 1,4-butanediol as a chain extender, and the precursor polymer, P. These analyses were performed under uniaxial stretching to evaluate their suitability for controlled drug delivery systems**. (Figure 4.4. a).**The elastic modulus, a reflection of a material's stiffness and ability to recover its shape after deformation, was markedly low in P-L at 0.647 KPa, contrasting sharply with REF (7 KPa) and P (111 KPa). This suggests

that incorporating LDH significantly reduces the stiffness of the polyurethane matrix. Tensile strength, measuring the maximum stress a material can endure before breaking, revealed a similar trend. P-L exhibited a tensile strength of 75 KPa, notably lower than P (2281 KPa) and REF (360 KPa), implying that P-L is a highly flexible and deformable material. A remarkable feature of P-L is its elongation at break, denoting the extent to which the material can stretch before breaking. P-L demonstrated an extraordinary elongation at break of 1230%, far exceeding P (34%) and REF (56%). This exceptional stretchability renders P-L ideal for applications where flexibility and adaptability are crucial. Furthermore, toughness, which measures the energy absorbed by the material before rupture, was significantly enhanced in P-L. It demonstrated a toughness of 770 kJ/m^3, superior to REF (100 kJ/m^3) and P (630 kJ/m^3), indicating that grafting LDH onto the polyurethane matrix enhances its resilience against impact and mechanical stress. Interestingly, the physical mixture of prepolymer and LDH (P-L physical) exhibited an elongation at break (33%) nearly identical to that of P (34%), suggesting a similar degree of flexibility. However, its elastic modulus (69 KPa), tensile strength (1969 KPa), and toughness (330 kJ/m^3) were more aligned with P than P-L (chemical), supporting the successful grafting of LDH onto the prepolymer backbone via functional modification. These mechanical characteristics are essential for applications like controlled drug delivery, where the material must endure mechanical stresses during implantation and operation within the body. The substantial elongation at break ensures that P-L can conform to complex geometries and movements in vivo without compromising mechanical integrity. The enhancement in elongation at break and toughness, driven by adding nanofillers like Li-Al LDH, has been previously observed with other fillers and extenders[42-44], such as CNT[45], graphene[46], boron nitride[47], ZnO[48], TiO_2[49], and halloysite[50]; yet none have achieved the remarkable increase in stretchability seen in P-L, which exhibits a 36-

fold improvement in elongation compared to its precursor polymer, P. The incorporation of Li-Al LDH in polyurethane significantly modifies its mechanical performance, making it a promising candidate for biomedical applications like controlled drug delivery, where it must withstand mechanical forces while effectively encapsulating and releasing therapeutic agents over time.

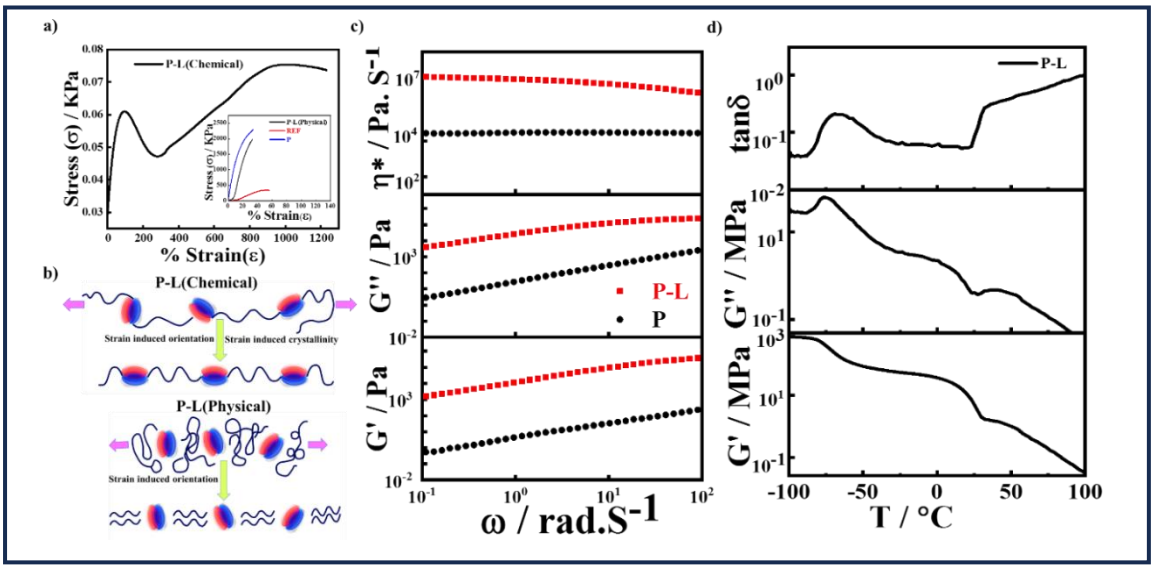

Figure 4.4: Some important characteristics of the designed nanocomposite include: **a)** Stress-strain charts illustrating the strengths of distinct nanocomposites, specifically polyurethane prepolymer grafted with Li-Al based LDH, referred to as P-L (chemical). The comparative stress-strain curves are shown in the inset graph for polyurethane prepolymer (P), Li-Al based LDH nanocarrier physically mixed with prepolymer, designated P-L (Physical), and when 2-butanol chemically reacts with polyurethane prepolymer (REF); **b)** Schematic illustration comparing P-L (Chemical) and P-L (Physical): Understanding the Dynamics Behind the Stress-Strain Curves. The stress-strain curves of P-L (Chemical) and P-L (Physical) reveal essential material responses under tension, showcasing a remarkable

contrast in behaviour. P-L (Chemical), driven by strong covalent cross-linking, effectively absorbs and dissipates energy, resulting in a stress-strain curve that stretches far beyond conventional expectations. This increased elasticity and resilience yield an extraordinary strain percentage, reflecting the material's ability to deform significantly without fracture, showcasing its tenacity under stress. Conversely, P-L (Physical), while resilient, derives its strength from weaker, reversible interactions such as hydrogen bonds or van der Waals forces. As observed in polyurethane prepolymer, these physical cross-links demonstrate a more limited deformation before yielding to stress, resulting in a controlled stress-strain curve with lower strain values. The difference in strain extent between these two systems lies in the bonding nature: P-L (Chemical) exhibits a passionate, nearly limitless stretch, while P-L (Physical) reflects a more restrained, practical performance. This fundamental divergence illustrates why P-L (Chemical) is distinguished by its remarkable strain capacity, while P-L (Physical), although stable, remains conservative in its elastic limits. **c)** Rheological insights into polyurethane prepolymer (P) and the prepolymer-grafted Li-Al LDH nanocomposite (P-L) at 160°C. At the elevated temperature of 160°C, the rheological behavior of polyurethane prepolymer (P) and its nanocomposite counterpart, where Li-Al based LDH is grafted onto the prepolymer matrix (P-L)(Fig 4.4.c), reveals a complex interaction of molecular dynamics. The heat activates polymer chain mobility in the prepolymer (P), facilitating a deeper exploration of its viscoelastic properties, such as shear thinning, relaxation, and flow characteristics. Meanwhile, the presence of the Li-Al nanofiller within the composite (P-L) enhances mechanical strength and thermal stability by introducing a hybrid nanostructure that resists deformation. The synergy between the polymer matrix and the LDH at this temperature unveils a fascinating realm of tunable viscoelasticity, viscosity reduction, and improved mechanical performance, presenting potential for advanced materials engineering. **d)** Understanding DMA of the novel

nanocomposite (P-L) and its glass transition temperature. DMA serves as a crucial tool in revealing the complex mechanical behaviour of materials, particularly in nanocomposites. In studying the novel nanocomposite (P-L), DMA provides significant insights into its viscoelastic properties, illuminating the material's response to stress, strain, and frequency variations across a temperature range. One of the most critical revelations from DMA is the glass transition temperature (Tg) of the nanocomposite. This temperature marks a crucial threshold where the material transitions from a rigid, glassy state to a more flexible, rubbery phase. For (P-L), understanding this shift reveals not only its thermal stability but also its potential for various applications where mechanical resilience and adaptability are essential. The Tg signifies the onset of molecular motion within the matrix, with the nanoscale reinforcements in (P-L) playing a vital role in modulating this behaviour.

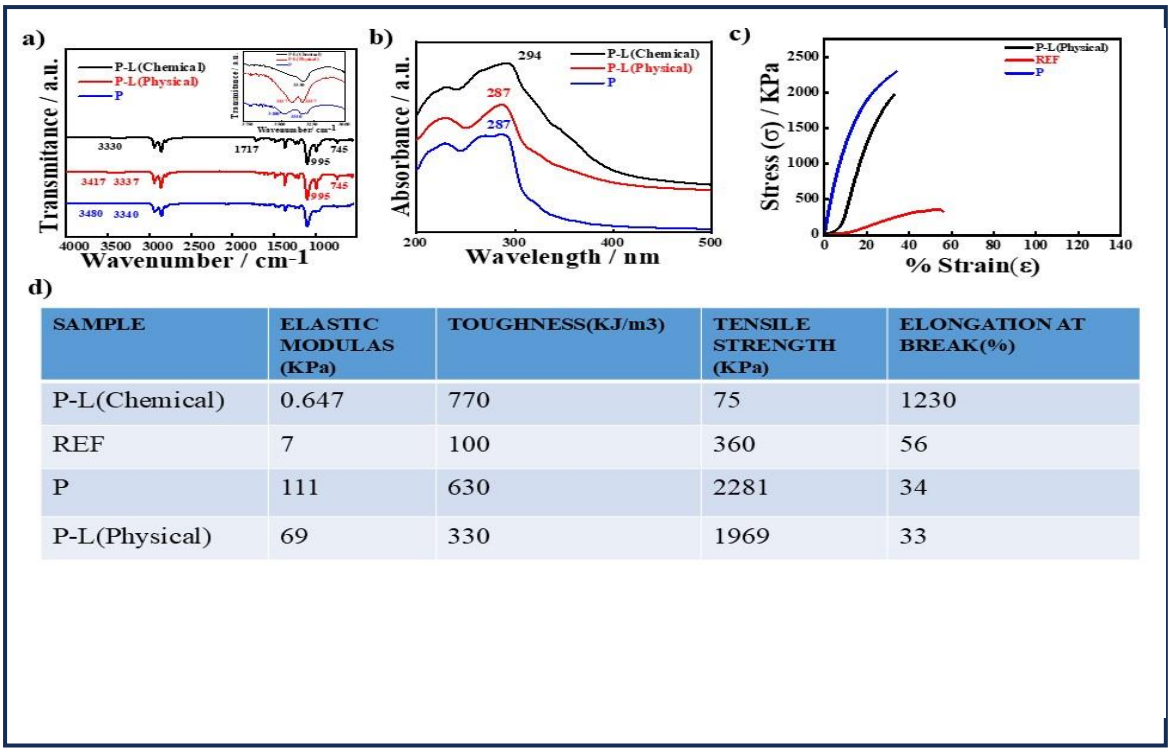

d)

SAMPLE	ELASTIC MODULAS (KPa)	TOUGHNESS(KJ/m3)	TENSILE STRENGTH (KPa)	ELONGATION AT BREAK(%)
P-L(Chemical)	0.647	770	75	1230
REF	7	100	360	56
P	111	630	2281	34
P-L(Physical)	69	330	1969	33

Figure 4.5:a) FTIR spectra of P-L chemical ,P-L (physical) and pure P. b) UV-VIS spectra of P-L chemical ,P-L (physical) and pure P. c)Stress strain plot of of P-L chemical ,P-L (physical) and pure P. d)Mechanical parameters of P-L chemical ,P-L (physical) , pure P and reference molecule.

The rheological properties of both P and P-L were examined to understand how grafting influences the viscoelastic characteristics of these materials. The analysis covered a frequency range of 0.1 to 100 radians per second at temperatures of 100°C, 120°C, 140°C, 160°C, and 180°C **(Figure 4.6.a and 4.6.c)**. The results provided valuable insights into the effects of LDH grafting on polyurethane. Both P and P-L displayed typical polymer behavior, characterized by a decrease in storage modulus (G'), loss modulus (G''), and complex viscosity (η*) with rising temperature. This trend is consistent with general polymer behavior, where increased temperatures enhance molecular mobility, thereby

reducing stiffness and viscosity. However, a notable distinction emerged between P and P-L. For the polyurethane (P), the rheological curves at varying temperatures were significantly spaced apart, indicating a higher sensitivity to temperature changes. Conversely, the curves for P-L remained much closer together across the same temperature range, suggesting that the presence of grafted LDH improves the thermal stability of the material's viscoelastic properties [51]. The LDH grafting in the P-L nanocomposite inhibited the relaxation process within the polymer matrix. The inclusion of LDH not only increased the rigidity of P-L but also stabilized the polymer structure. This stabilization is evident in the consistently higher storage modulus, loss modulus, and complex viscosity of P-L compared to P at all measured temperatures, particularly pronounced at 160°C. Throughout most of the frequency range, P-L exhibited superior storage modulus, loss modulus, and complex viscosity than P. The elevated storage modulus (G') in P-L signifies a stiffer material with enhanced resistance to deformation, while the higher loss modulus (G") indicates increased energy dissipation, likely due to interactions between the LDH and the polyurethane matrix. Furthermore, the complex viscosity (η*) of P-L exceeded that of P at the same temperature, highlighting the influence of grafted LDH on flow resistance. This enhanced viscosity suggests greater structural integrity and a more resilient polymer network, resulting from the reinforcing effects of LDH particles. In summary, the grafting of LDH onto polyurethane significantly modifies its rheological properties, enhancing both rigidity and thermal stability. These improvements in viscoelastic behaviour highlight the potential of LDH-grafted polyurethane for applications requiring precise material control and superior performance.

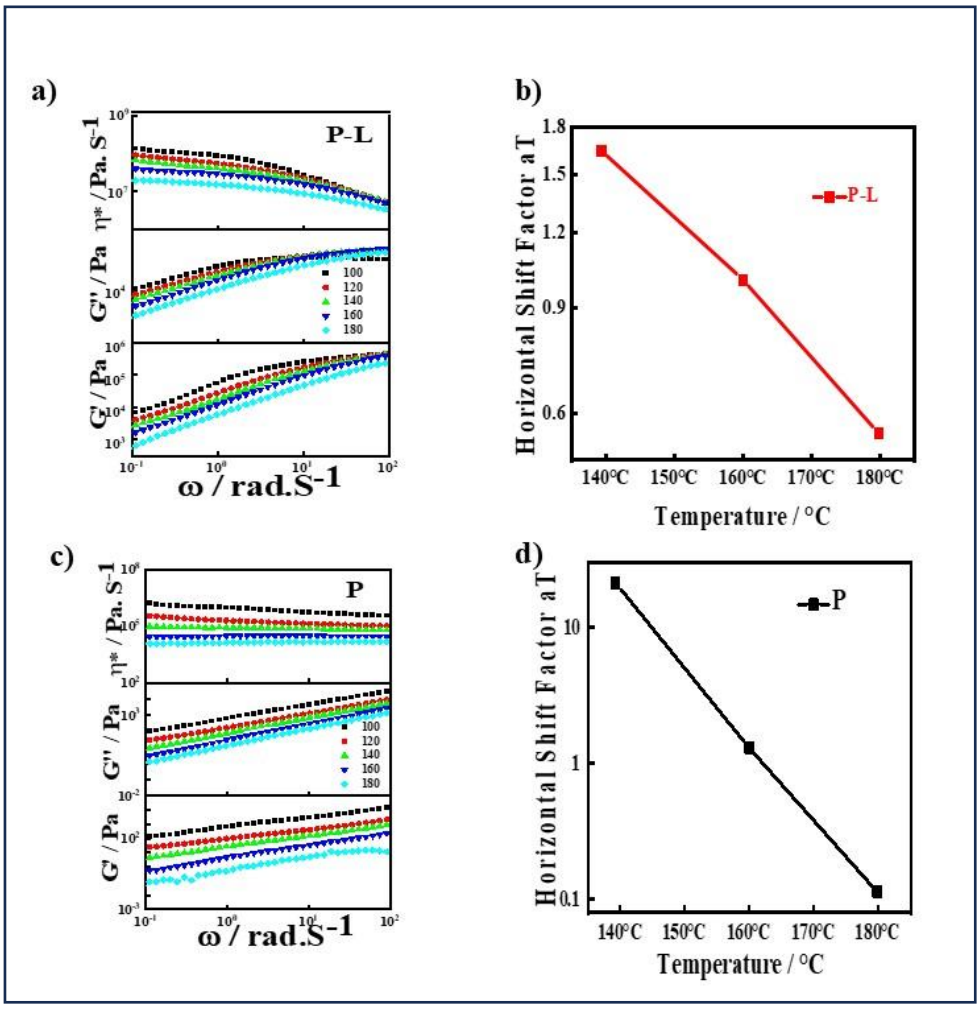

Figure 4.6: Temperature modulated Rheological behaviour of P and P-L

In our DMA of the polyurethane grafted Li-Al based LDH nanocomposite (P-L), we identified two distinct relaxation temperatures: -68°C and 33°C. **(Figure 4.4.d)** These temperatures reflect unique relaxation behaviours within the material. The first relaxation temperature of -68°C aligns with the glass transition temperature (Tg) of the polyurethane matrix. At this point, the polymer chains exhibit rigidity and limited mobility, resulting in a higher storage modulus and a lower loss modulus. As the temperature increases, the chains become more flexible, leading to a peak in the tan delta curve, indicating enhanced molecular relaxation and energy dissipation as the material transitions into a more rubbery state. The second relaxation temperature of 33°C likely corresponds to a secondary

transition or the influence of the P-L nanocomposite. This temperature may reflect changes at the interface between the polyurethane and the LDH particles, impacting the local mobility of the polymer chains and altering the composite's mechanical behavior. Throughout the temperature range of -100°C to 100°C, both storage moduli gradually decline, indicating typical polymer behavior as they transition from a glassy to a rubbery state, becoming softer and more flexible with rising temperature.[52,53] These observations underscore the pivotal role of LDH in influencing the thermal and mechanical properties of the polyurethane matrix.

4.2.4. Encapsulation and sustained release profile of Dox in Polyurethane grafted Li-Al based LDH nanocomposite:

The polyurethane grafted Li-Al based LDH nanocomposite, recognized for its exceptional mechanical strength, thermal stability, and self-assembling nanostructures, has emerged as a promising candidate for drug delivery and implants. Its distinctive properties make it particularly well-suited for sustained drug release, which is crucial for maintaining controlled drug concentrations in the bloodstream over extended periods. This capability not only enhances the drug's efficacy but also reduces the risk of side effects. As shown in Fig 4.7.a, the cumulative release profile of doxorubicin, a model anti-cancer drug, from the nanocomposite exhibits significant improvement compared to the pristine polyurethane system, highlighting its potential in advanced medical applications.

The chemotherapeutic efficacy of the anti-cancer drug doxorubicin (Dox) relies heavily on its sustained release, closely linked to the design of its carrier and the effective release from polyurethane grafted Li-Al based LDH nanocomposite. In this study, we investigated the release behavior of Dox from two systems, P@Dox and P-L@Dox, under biomimetic conditions using buffer solutions and external stimuli such as pH. Release was monitored

by measuring UV absorbance at 480 nm from the supernatant. After 80 hours of incubation in PBS at pH ~7.4, the release rates were 15% for P@Dox and 5% for P-L@Dox **(Figure.4.7.a),** demonstrating a slow, sustained cumulative release. Notably, DOX@LDH3 showed superior sustained release, attributed to its more stable grafted layered structure and stronger hydrogen bonding, enabling better encapsulation of Dox molecules compared to the initial burst release observed with the P@Dox system.**(Figure 4.7.a)**

Additionally, we explored pH-dependent drug release to simulate the acidic environment of tumor tissue. After 80 hours, significantly higher release percentages of 20% and 33% were recorded at pH 6 and pH 4, respectively **(Figure.4.7.b)**. This marked increase in drug release at lower pH underscores the potential for targeted drug delivery in acidic tumor environments, contrasting with minimal drug release in normal tissues (pH > 6). Importantly, P-L@Dox exhibited a remarkable ability to preferentially deliver the drug to tumor tissue, with 33% delivery at acidic pH compared to just 5% at neutral pH. This responsiveness indicates that the P-L@Dox formulation effectively simulates the endosomal and lysosomal environment, enhancing targeted drug delivery. Sustained drug release is particularly vital for cancer treatment, as it helps maintain therapeutic drug concentrations over extended periods, minimizing severe side effects.

While many organic and inorganic nanoparticles are susceptible to hydrolysis even under neutral conditions, our findings indicate that the polyurethane grafted Li-Al based LDHs nanocomposite offers enhanced resistance to acidic degradation, making it a promising drug delivery vehicle. The complex drug release mechanism involves multiple factors, including drug diffusion from the nanocarrier matrix and solvent penetration into the matrix, which collectively regulate the kinetics of drug release. To gain deeper insights into the release mechanism, we applied various kinetic models to the P@Dox and P-L@Dox systems, including zero-order, first-order, Higuchi, and Korsmeyer-Peppas models

(Supplementary Fig. S). The correlation coefficients (r^2) indicated that the Higuchi and Korsmeyer-Peppas models provided the best fit for the P-L@Dox system, with r^2 values of 0.98 and 0.96, respectively. The release exponent (n), reflecting the drug's transport mechanism, was 0.23 for P@Dox and 0.33 for P-L@Dox, suggesting a quasi-Fickian diffusion process with non-swellable matrix diffusion. From the in vitro drug release studies, it becomes evident that the drug's release is both controlled and gradual. This behavior is primarily due to the hydrophobic polyurethane chains surrounding the hydrophilic layered double hydroxide backbone, together forming a tortuous path enhanced by interactive dynamics, ensuring a measured and sustained release.(Fig 4.8. a,b,c,d)

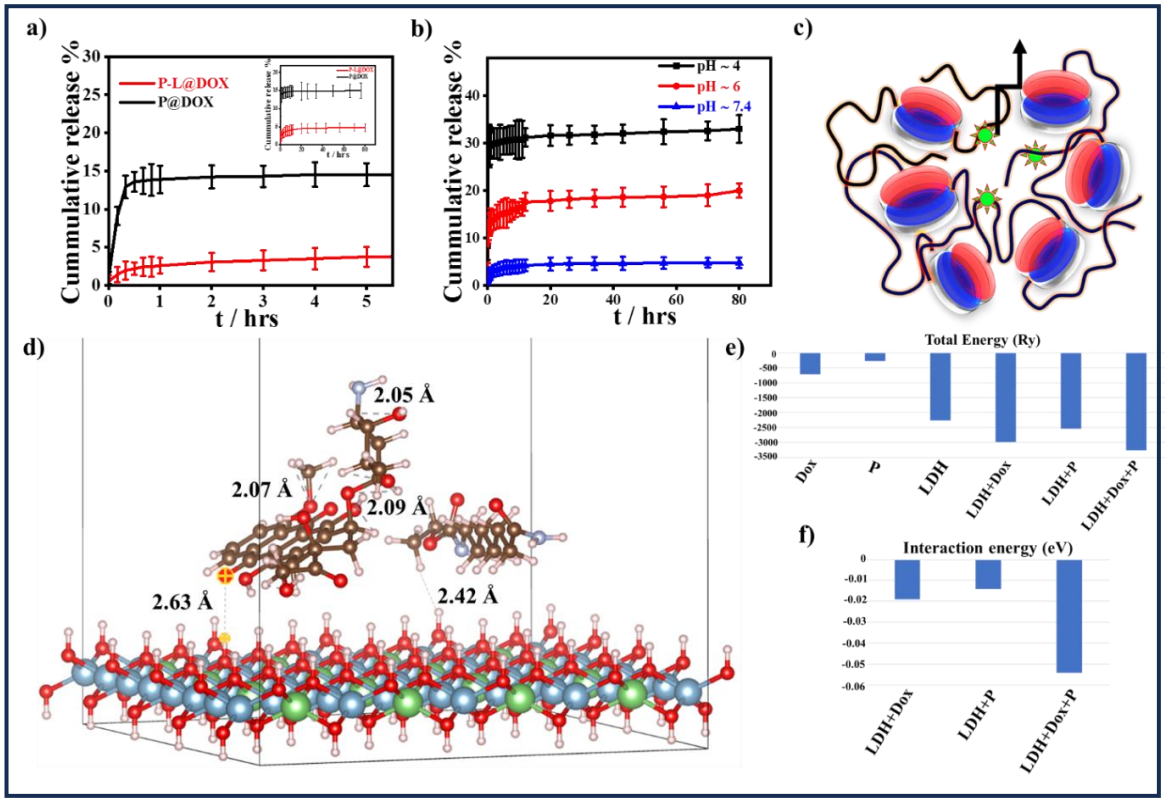

Figure 4.7: The pH-triggered drug release from the formulation is governed by robust interactions between doxorubicin (Dox) and prepolymer grafted Li-Al LDH nanocomposites, ensuring a thermodynamically regulated, controlled, and sustained release. **a)** A comparison of the cumulative drug release profiles for the prepolymer and grafted nanocomposite loaded with Dox (P@Dox and P-L@Dox) in PBS at 37 °C and

approximately pH 7.4 shows that the stronger connections and larger confinement of the novel nanocomposite, P-L@Dox, facilitate continuous sustained drug release, whereas the prepolymer loaded Dox system (P@Dox) exhibits a burst release of the drug. **b)** Comparative release profiles of Dox in PBS at various pH levels (approximately 7.4, 6, and 4 at 37 °C) from the P-L@Dox formulation are illustrated. Data is presented as mean value ± SD (n = 3). **c)** A schematic illustration depicts the mechanism of medication release from the designed nanocomposite architecture. **d)** The configuration of interactions between the Dox molecule and the prepolymer grafted Li-Al based LDH nanocomposite, highlighting the corresponding hydrogen bonding. **e)** Variation in the total energy of all components involved in the design of the nanocomposite and the novel formulation is presented, with colour coding: blue for Aluminium, green for Lithium, red for Oxygen, white for Hydrogen, and black for Carbon. **f)** The interaction energy variations for the LDH+Dox, LDH+P, and LDH+P+Dox systems are analyzed to understand the thermodynamic efficiency and potential for formulating effective nanocomposites.

4.2.5. Theoretical Understanding of Interaction through Thermodynamics and Mechanical Response:

The crystal structure of LDH (Li1-x AlxOH) was intricately designed by incorporating aluminium atoms into the lithium hydroxide crystal lattice at varying concentrations. The intrinsic structure of LiOH showcases a tetragonal arrangement and belongs to the P4/nmm space group, characterized by lattice parameters of a = 4.93 Å, b = 4.94 Å, and c = 4.28 Å. According to the Materials Project database [56], the LiOH crystal consists of a single LiOH sheet oriented along the (0, 0, 1) plane. Here, each Li+ ion is bonded to four

equivalent O2- atoms, forming a complex arrangement of distorted corner- and edge-sharing LiO_4 tetrahedra, with Li–O bond lengths consistently measured at 1.94 Å. Each H+ ion forms a singular bond with an O^{2-} ion, yielding an H–O bond length of 0.96 Å, while the O2- atoms link in a distorted single-bond geometry to four equivalent Li+ ions and one H+ ion, creating a harmonious lattice structure.

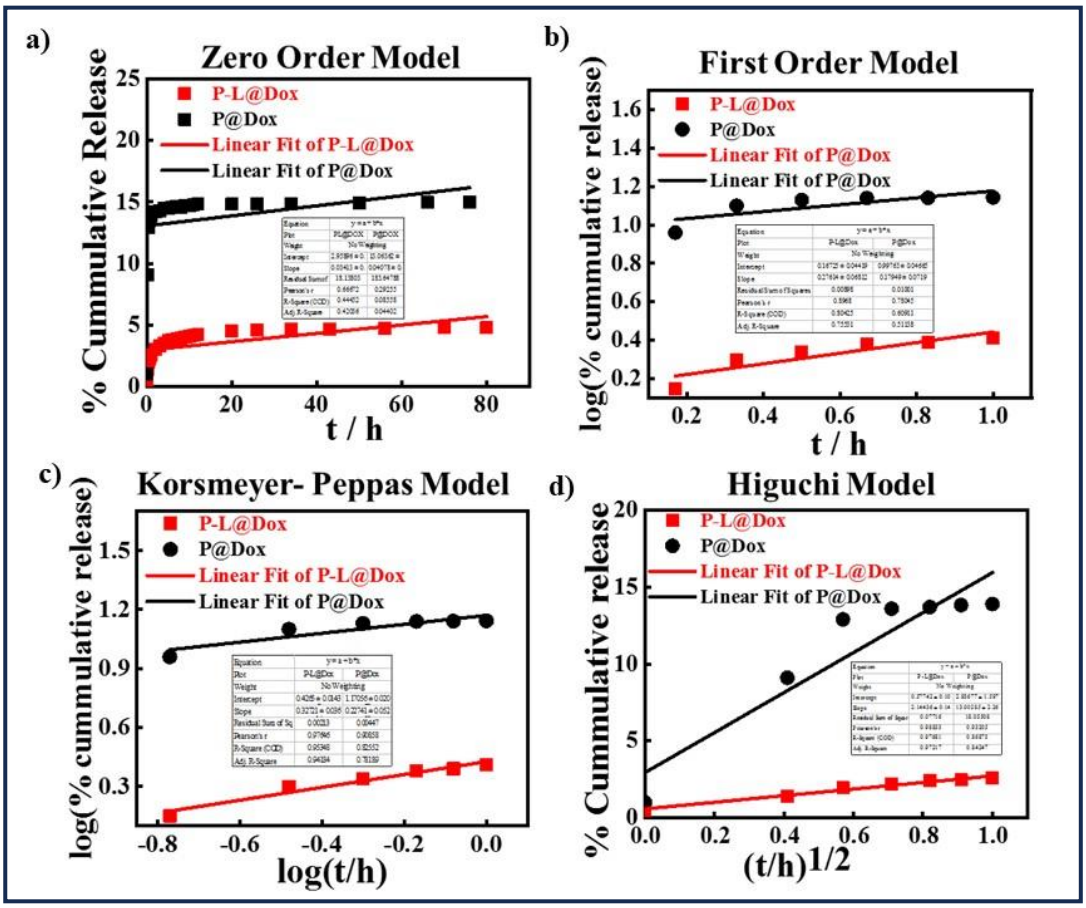

Fig 4.8. Different kinetic model of controlled drug release. a) Zero order Model, b)First order model, c)Korsmeyer- Peppas Model. d) Higuchi model.

To achieve the desired concentration of Al in the lattice, 4x4x1 monolayer supercells were constructed, allowing for expanded interlayer spacing to accommodate the doxorubicin

(Dox) molecule. The stability and interaction of the LDH-Dox complex were evaluated by optimizing vacuum distances of 10, 15, and 20 Å, with the 15 Å vacuum being chosen to effectively prevent interaction with its mirror image due to the inherent symmetry. Subsequent relaxation calculations indicated that this configuration resulted in a highly stable intercalated system, characterized by the lowest total ground-state energy. As depicted in Figure 1, the doxorubicin molecule—comprising C, H, N, and O atoms and measuring approximately 15 Å in length and 11 Å in width—aligns nearly parallel to the LDH sheet. This orientation is driven by intramolecular forces between adjacent O and H atoms within the doxorubicin molecule, enabling it to nestle within the confined space and form a stable complex. The presence of strong hydrogen bonds within Dox, along with weaker interactions between Dox and the LDH system, highlights the robustness of the intercalation. These bonds are crucial for ensuring the slow and controlled release of the drug, positioning the LDH-Dox system as a promising candidate for targeted therapeutic applications.

From a thermodynamic standpoint, the free energy of a system is significantly influenced by its enthalpy (H) and entropy (S), as expressed by the equation: G = H - TS, where T represents the system's temperature in Kelvin (K). This relationship elegantly underscores how energy and disorder dictate the stability and behavior of a system. From our calculations of the relaxed intercalated systems, the total energy, F, comprises four distinct contributions: the one-electron energy, the Hartree energy, the exchange-correlation energy, and the Ewald energy, expressed as F = E - TS, with E representing the internal energy where E = F + TS. These relationships reveal the intricate balance between various energy forms, each contributing to the overall thermodynamic properties of the system.

In the context of drug carriers, thermodynamic properties are pivotal in determining the stability and mobility of drug molecules. The presence of a polymer within the system generates a significant negative enthalpy and total energy, calculated using density functional theory (DFT). This results in negative free energy, strongly indicating the stability and spontaneous nature of the surface-modified LDH-drug intercalation process. The doping of Al^{3+} cations in the 4x4 LiOH supercells was limited to less than 10% to prevent cluster fragmentation and ensure a uniform bond distribution. Under the basic conditions expected in the LDH-Dox system, charge neutrality was intentionally avoided, maintaining the LDH component with a positive charge. Typically, this charge would be balanced by counter ions like nitrate or chloride; however, to reduce computational costs in large quantum mechanical calculations, external anions were excluded. It was assumed that the necessary excess electrons would be provided by the drug molecule itself.

As demonstrated and supported by prior studies [, increasing the concentration of Al in the system significantly enhances the stability and intercalation efficiency of doxorubicin (Dox) compared to the pure LiOH-Dox system. The conformational changes of the Dox molecule when influenced by the polymer, resulting in a more stable configuration with lower ground state energy than the pristine Dox molecule. This enhanced intercalation, evidenced by an increased number of hydrogen bonds within the Dox molecule, indicates that the polymer's presence fosters greater intramolecular hydrogen bonding while reducing intermolecular interactions. Consequently, the polymer-containing system exhibits more controlled drug release and uptake compared to the polymer-free system.

While DFT provides accurate quantum mechanical insights, it becomes computationally expensive and time-consuming for large systems, such as bulk materials or complex drug carriers. DFT scales poorly with system size, rendering it impractical for extensive simulations involving thousands of atoms or large drug delivery vehicles. Conversely, CHGNet utilizes machine learning to model atomic interactions efficiently and handle large systems more effectively. Trained on extensive material databases, CHGNet can swiftly predict mechanical properties in a fraction of the time required for DFT calculations.

For large-scale bulk systems like polymer matrices, nanoparticle assemblies, or complex biological carriers, CHGNet's capacity to process extensive datasets and model material behavior at scale presents a significant advantage. Its graph neural network architecture excels in capturing long-range interactions and complex atomic structures without the need for intensive quantum mechanical calculations, making it ideal for predicting the mechanical properties of large drug carriers. While DFT generally necessitates recalculations for each new material or structure, CHGNet can generalize across diverse material classes once trained on a sufficiently large and varied dataset. This adaptability allows it to provide quick insights into the mechanical behavior of new materials without starting from scratch, as would be required with DFT. CHGNet's machine learning framework enables it to learn patterns from large databases, such as the Materials Project or other experimentally generated datasets, allowing predictions not only of mechanical properties but also of other related factors such as stability, degradation, and modification potential, which are vital for drug vehicle design. In contrast, DFT primarily focuses on electronic structure and necessitates additional calculations for mechanical predictions, limiting its speed and adaptability.**(Fig 4.7. c,d,e,f)**

4.3 Conclusion

In summary, CHGNet presents a highly efficient, scalable, and flexible approach to predicting the mechanical properties of drug delivery vehicles. It facilitates faster and more cost-effective simulations for large and complex systems, accelerating the design and optimization of materials for therapeutic applications. While DFT remains invaluable for detailed electronic insights, CHGNet provides a practical and powerful alternative for predicting large-scale mechanical properties, especially when speed and scalability are priorities, making it indispensable for our study. The elastic (E), bulk (K), and shear modulus (G) predicted by the ML-trained CHGNet potential are key mechanical properties that describe the structural integrity and physical response to external deformation of both the pristine polymer and the polymer grafted LDH system. Additionally, the predicted modulus properties have been referenced against commonly available systems such as PE and PP for validation. A notable contrast is observed in the significant decrease in the elasticity of the LDH intercalated system with increasing Al% concentration, which can again be attributed to the relative increase in strain due to a rise in positive charge and weakened bonding within the LiAl LDH system.

4.4. References:

1) Bray, F., Laversanne, M., Sung, H., Ferlay, J., Siegel, R. L., Soerjomataram, I., & Jemal, A. (2024). Global cancer statistics 2022: GLOBOCAN estimates of incidence and mortality worldwide for 36 cancers in 185 countries. *CA: a cancer journal for clinicians*, *74*(3), 229-263.
2) Hubbell, J. A., & Chilkoti, A. (2012). Nanomaterials for drug delivery. *Science*, *337*(6092), 303-305.
3) Thakor, A. S., & Gambhir, S. S. (2013). Nanooncology: the future of cancer diagnosis and therapy. *CA: a cancer journal for clinicians*, *63*(6), 395-418.
4) Chen, Z., Han, F., Du, Y., Shi, H., & Zhou, W. (2023). Hypoxic microenvironment in cancer: molecular mechanisms and therapeutic interventions. *Signal transduction and targeted therapy*, *8*(1), 70.
5) Anand, U., Dey, A., Chandel, A. K. S., Sanyal, R., Mishra, A., Pandey, D. K., ... & de la Lastra, J. M. P. (2023). Cancer chemotherapy and beyond: Current status, drug candidates, associated risks and progress in targeted therapeutics. *Genes & Diseases*, *10*(4), 1367-1401.
6) Lee, Y. H., & Chen, C. S. (2024). Carcinomembrane-Camouflaged Perfluorochemical Dual-Layer Nanopolymersomes Bearing Indocyanine Green and Camptothecin Effectuate Targeting Photochemotherapy of Cancer. *ACS Biomaterials Science & Engineering*.
7) Ladewig, K., Xu, Z. P., & Lu, G. Q. (2009). Layered double hydroxide nanoparticles in gene and drug delivery. *Expert Opinion on Drug Delivery*, *6*(9), 907-922.
8) Oh, J. M., Choi, S. J., Lee, G. E., Han, S. H., & Choy, J. H. (2009). Inorganic drug-delivery nanovehicle conjugated with cancer-cell-specific ligand. *Advanced Functional Materials*, *19*(10), 1617-1624.

9) Mok, H., Park, J. W., & Park, T. G. (2008). Enhanced intracellular delivery of quantum dot and adenovirus nanoparticles triggered by acidic pH via surface charge reversal. *Bioconjugate chemistry*, *19*(4), 797-801.

10) Singh, A. P., Biswas, A., Shukla, A., & Maiti, P. (2019). Targeted therapy in chronic diseases using nanomaterial-based drug delivery vehicles. *Signal transduction and targeted therapy*, *4*(1), 33.

11) He, C., Kim, S. W., & Lee, D. S. (2008). In situ gelling stimuli-sensitive block copolymer hydrogels for drug delivery. *Journal of controlled release*, *127*(3), 189-207.

12) Darr, J. A., Zhang, J., Makwana, N. M., & Weng, X. (2017). Continuous hydrothermal synthesis of inorganic nanoparticles: applications and future directions. *Chemical reviews*, *117*(17), 11125-11238.

13) Ni, D., Bu, W., Ehlerding, E. B., Cai, W., & Shi, J. (2017). Engineering of inorganic nanoparticles as magnetic resonance imaging contrast agents. *Chemical Society Reviews*, *46*(23), 7438-7468.

14) Kwon, H. J., Shin, K., Soh, M., Chang, H., Kim, J., Lee, J., ... & Hyeon, T. (2018). Large-scale synthesis and medical applications of uniform-sized metal oxide nanoparticles. *Advanced Materials*, *30*(42), 1704290.

15) Beach, M. A., Nayanathara, U., Gao, Y., Zhang, C., Xiong, Y., Wang, Y., & Such, G. K. (2024). Polymeric Nanoparticles for Drug Delivery. *Chemical Reviews*, *124*(9), 5505-5616.

16) Pavlidou, S., & Papaspyrides, C. D. (2008). A review on polymer–layered silicate nanocomposites. *Progress in polymer science*, *33*(12), 1119-1198.

17) Wang, Q., Wu, J., Gao, Y., Zhang, Z., Wang, J., Zhang, X., ... & O'Hare, D. (2013). Polypropylene/Mg 3 Al–tartrazine LDH nanocomposites with enhanced thermal

stability, UV absorption, and rheological properties. *RSC advances*, *3*(48), 26017-26024.

18) Guo, S., Zhang, C., Peng, H., Wang, W., & Liu, T. (2011). Structural characterization, thermal and mechanical properties of polyurethane/CoAl layered double hydroxide nanocomposites prepared via in situ polymerization. *Composites Science and Technology*, *71*(6), 791-796.

19) He, F. A., & Zhang, L. M. (2007). New polyethylene nanocomposites prepared by in-situ polymerization method using nickel a-diimine catalyst supported on organo-modified ZnAl layered double hydroxide. *Composites Science and Technology*, *67*(15-16), 3226-3232.

20) Bao, Y. Z., Huang, Z. M., & Weng, Z. X. (2006). Preparation and characterization of poly (vinyl chloride)/layered double hydroxides nanocomposite via in situ suspension polymerization. *Journal of applied polymer science*, *102*(2), 1471-1477.

21) Shin, S. Y. A., Simon, L. C., Soares, J. B., & Scholz, G. (2003). Polyethylene–clay hybrid nanocomposites: in situ polymerization using bifunctional organic modifiers. *Polymer*, *44*(18), 5317-5321.

22) Manias, E., Touny, A., Wu, L., Strawhecker, K., Lu, B., & Chung, T. C. (2001). Polypropylene/montmorillonite nanocomposites. Review of the synthetic routes and materials properties. *Chemistry of Materials*, *13*(10), 3516-3523.

23) Zhang, H., Zhang, J., Yun, R., Jiang, Z., Liu, H., & Yan, D. (2016). Nanohybrids of organo-modified layered double hydroxides and polyurethanes with enhanced mechanical, damping and UV absorption properties. *RSC advances*, *6*(41), 34288-34296.

24) Ferrero, C., Bravo, I., & Jiménez-Castellanos, M. R. (2003). Drug release kinetics and fronts movement studies from methyl methacrylate (MMA) copolymer matrix tablets:

effect of copolymer type and matrix porosity. *Journal of controlled release*, *92*(1-2), 69-82.

25) Peppas, N. A., & Langer, R. (1994). New challenges in biomaterials. *Science*, *263*(5154), 1715-1720.

26) Lendlein, A., & Langer, R. (2002). Biodegradable, elastic shape-memory polymers for potential biomedical applications. *Science*, *296*(5573), 1673-1676.

27) Lendlein, A., Jiang, H., Jünger, O., & Langer, R. (2005). Light-induced shape-memory polymers. *Nature*, *434*(7035), 879-882.

28) Biswas, A., Aswal, V. K., Ray, B., & Maiti, P. (2018). Nanostructure-controlled shape memory effect in polyurethanes. *The Journal of Physical Chemistry C*, *122*(20), 11167-11176.

29) Biswas, A., Aswal, V. K., Sastry, P. U., Rana, D., & Maiti, P. (2016). Reversible bidirectional shape memory effect in polyurethanes through molecular flipping. *Macromolecules*, *49*(13), 4889-4897.

30) Zhou, L., Yu, L., Ding, M., Li, J., Tan, H., Wang, Z., & Fu, Q. (2011). Synthesis and characterization of pH-sensitive biodegradable polyurethane for potential drug delivery applications. *Macromolecules*, *44*(4), 857-864.

31) Petrini, P., Tanzi, M. C., Moran, C. R., & Graham, N. B. (1999). Linear poly (ethylene oxide)-based polyurethane hydrogels: polyurethane-ureas and polyurethane-amides. *Journal of Materials Science: Materials in Medicine*, *10*, 635-639.

32) Shukla, A., Singh, A. P., Dubey, T., Hemalatha, S., & Maiti, P. (2019). Third generation cyclodextrin graft with polyurethane embedded in hydrogel for a sustained drug release: complete shrinkage of melanoma. *ACS Applied Bio Materials*, *2*(4), 1762-1771.

33) Shukla, A., Singh, A. P., & Maiti, P. (2021). Injectable hydrogels of newly designed brush biopolymers as sustained drug-delivery vehicle for melanoma treatment. *Signal Transduction and Targeted Therapy*, *6*(1), 63.

34) Kotal, M., & Srivastava, S. K. (2011). Synergistic effect of organomodification and isocyanate grafting of layered double hydroxide in reinforcing properties of polyurethane nanocomposites. *Journal of Materials Chemistry*, *21*(46), 18540-18551.

35) Patel, D. K., Gupta, V., Dwivedi, A., Pandey, S. K., Aswal, V. K., Rana, D., & Maiti, (2016). Superior biomaterials using diamine modified graphene grafted polyurethane. *Polymer*, *106*, 109-119.

36) Guo, S., Zhang, C., Peng, H., Wang, W., & Liu, T. (2011). Structural characterization, thermal and mechanical properties of polyurethane/ CoAl layered double hydroxide nanocomposites prepared via in situ polymerization. *Composites Science and Technology*, *71*(6), 791-796.

37) Starukh, G., Budzinska, V., & Brychka, S. Y. (2019). Structural characterization, thermal and mechanical properties of polyurethane–MgAl–layered double hydroxide nanocomposites prepared via physical dispersion. *Applied Nanoscience*, *9*, 987-996.

38) Naseem, S., Lonkar, S. P., Leuteritz, A., & Labuschagné, F. J. W. (2018). Different transition metal combinations of LDH systems and their organic modifications as UV protecting materials for polypropylene (PP). RSC advances, 8(52), 29789-29796.

39) Li, S., Amat, D., Peng, Z., Vanni, S., Raskin, S., De Angulo, G., ... & Leblanc, R. M. (2016). Transferrin conjugated nontoxic carbon dots for doxorubicin delivery to target pediatric brain tumor cells. Nanoscale, 8(37), 16662-16669.

40) Shukla, A., Singh, A. P., Ray, B., Aswal, V., Kar, A. G., & Maiti, P. (2019). Efficacy of polyurethane graft on cyclodextrin to control drug release for tumor treatment. *Journal of colloid and interface science*, *534*, 215-227.

41) Shukla, A., Maity, S., Ray, B., & Maiti, P. (2021). Dextrin and polyurethane graft copolymers as drug carrier: synthesis, characterization, drug release, biocompatibility and in-vitro toxicity. *Carbohydrate Polymer Technologies and Applications*, *2*, 100171.

42) Patel, D. K., Gupta, V., Dwivedi, A., Pandey, S. K., Aswal, V. K., Rana, D., & Maiti, P. (2016). Superior biomaterials using diamine modified graphene grafted polyurethane. *Polymer*, *106*, 109-119.

43) Patel, D. K., Rana, D., Aswal, V. K., Srivastava, S., Roy, P., & Maiti, P. (2015). Influence of graphene on self-assembly of polyurethane and evaluation of its biomedical properties. *Polymer*, *65*, 183-192.

44) Kumar, M. A., Vikas, M., Nitesh, S., Debabrata, D., Sudip, M., Mohan, K., & Pralay, M. (2015). Polyurethane-Grafted Chitosan as New Biomaterials for Controlled Drug Delivery.

45) Yang, Y., Li, X., Jiang, H., Ge, M., Su, X., Zou, M., & Li, G. (2023). Carbon nanotubes grafted by polyurethane chains with dopamine-mediation to enhance the mechanical and damping properties of polyurethane elastomer. *Polymer*, *280*, 126041.

46) Albozahid, M., Naji, H. Z., Alobad, Z. K., Wychowaniec, J. K., & Saiani, A. (2022). Thermal, mechanical, and morphological characterisations of graphene nanoplatelet/graphene oxide/high-hard-segment polyurethane nanocomposite: a comparative study. *Polymers*, *14*(19), 4224.

47) Bashir, A., Maqbool, M., Lv, R., Usman, A., Guo, H., Aftab, W., ... & Bai, S. L. (2021). Surface modified boron nitride towards enhanced thermal and mechanical performance of thermoplastic polyurethane composite. *Composites Part B: Engineering*, *218*, 108871.

48) Zahra, M., Ullah, H., Javed, M., Iqbal, S., Ali, J., Alrbyawi, H., ... & Somaily, H. H. (2022). Synthesis and characterization of polyurethane/zinc oxide nanocomposites with improved thermal and mechanical properties. *Inorganic Chemistry Communications*, *144*, 109916.

49) Król, P., Szlachta, M., & Pielichowska, K. (2022). Hydrophilic and hydrophobic films based on polyurethane cationomers containing TiO2 nanofiller. *Progress in Organic Coatings*, *162*, 106524.

50) Sun, J. T., Li, J. W., Tsou, C. H., Pang, J. C., Chung, R. J., & Chiu, C. W. (2020). Polyurethane/nanosilver-doped halloysite nanocomposites: Thermal, mechanical properties, and antibacterial properties. *Polymers*, *12*(11), 2729.

51) Costa, F. R., Wagenknecht, U., Jehnichen, D., Goad, M. A., & Heinrich, G. (2006). Nanocomposites based on polyethylene and Mg–Al layered double hydroxide. Part II. Rheological characterization. *Polymer*, *47*(5), 1649-1660.

52) Quijada-Garrido, I., Laterza, B., Mazón-Arechederra, J. M., & Barrales-Rienda, J. M. (2006). Characteristic features of chitosan/glycerol blends dynamics. *Macromolecular Chemistry and Physics*, *207*(19), 1742-1751.

53) Wan, Y., Wu, H., Yu, A., & Wen, D. (2006). Biodegradable polylactide/chitosan blend membranes. *Biomacromolecules*, *7*(4), 1362-1372.

54) Sadeghi, M., Semsarzadeh, M. A., Barikani, M., & Ghalei, B. (2011). Study on the morphology and gas permeation property of polyurethane membranes. *Journal of membrane science*, *385*, 76-85.

55) Costa, F. R., Saphiannikova, M., Wagenknecht, U., & Heinrich, G. (2008). Layered double hydroxide based polymer nanocomposites. *Wax Crystal Control· Nanocomposites· Stimuli-Responsive Polymers*, 101-168.

56) Ong, S. P., Richards, W. D., Jain, A., Hautier, G., Kocher, M., Cholia, S., ... & Ceder, G. (2013). Python Materials Genomics (pymatgen): A robust, open-source python library for materials analysis. *Computational Materials Science*, *68*, 314-3